

CosForce: A Force-Based General Model Considering Pedestrian Anticipation and Reaction Mechanisms

JINGHUI WANG¹ AND WEI LV^{1,2,*}

¹*School of Safety Science and Emergency Management
Wuhan University of Technology
Wuhan, China*

²*China Research Center for Emergency Management
Wuhan University of Technology
Wuhan, China*

ABSTRACT

In this study, a force-based general model, named the CosForce model, has been developed. To the best of our knowledge, this may represent the most simplified version of the force-based model. Considering the anisotropic interplay of pedestrians, the model focuses on binary interactions rather than metric-based interactions. Specifically, cosine functions are employed to describe the asymmetric interactions between the focal pedestrian and their nearest neighbor, implicitly simulating anticipation and reaction mechanisms.

In addition to numerical calibration in basic scenarios, the simulation primarily focuses on two intriguing crowd phenomena: "phase separation" and the "catfish effect". Speed related metrics are introduced to quantitatively analyze self-organizing phenomena, and the "catfish effect" is examined from the perspective of momentum assessment. Many of the results require further exploration, particularly with support from empirical data. This study provides a new perspective on pedestrian modeling: the dynamics among pedestrians can be simplified as binary interactions.

Keywords: agent-based models, collective dynamics, phase separation, catfish effect, numerical simulation

1. INTRODUCTION

The study of pedestrian dynamics modeling has undergone several decades of development. As a branch of collective dynamics, it has naturally integrated with fields such as multi-agent systems and robotic swarms, currently exhibiting unprecedented vitality. Microscopic pedestrian dynamics models primarily focus on crowd simulation driven by real-time pedestrian interactions. On a broader scale, additional rule sets can be incorporated to simulate mechanisms such as route choice in pedestrian traffic, etc (tactical level). Classic approaches, such as the cellular automaton model (Burstedde et al. 2001), the social force model (Helbing & Molnar 1995), the reciprocal velocity obstacles model (Van den Berg et al. 2008), the heuristic model (Moussaïd et al. 2011), and the PLE model (Guy et al. 2010) based on Maupertuis' Principle of Least Action, have been widely applied.

Due to their high extensibility, force-based models have been applied not only in pedestrian dynamics modeling but also in broader fields (Liu et al. 2024). New rule sets can be added by researchers to investigate specific mechanisms as required. Among these mechanisms, pedestrian anticipation and reaction have been extensively analyzed. Pedestrian reaction behaviors are generally viewed as passive responses to the environment, such as car-following behavior, whereas anticipation behaviors are considered active responses to environmental stimuli, such as a goalkeeper's predictive dive in soccer. A similar mechanism has been observed in experimental research within the field of cognitive science. Interactive experiments has revealed that visual attention is deployed differentially, depending on the nature of the behavioral goal that designates the task relevance of visual input (Renton et al. 2019; Frielink-Loing et al. 2017). The subtle distinctions between anticipation and reaction mechanisms are frequently overlooked, leading to the homogenization

* weil@whut.edu.cn (W. Lv)

of the modeling process. Collision avoidance rules can be introduced into force-based models in various forms, based on the relative velocity and relative distance of agents. Currently, the model incorporating collision avoidance rules based on the time-to-collision (TTC) potential is commonly regarded as the anticipation based model (Zanlungo et al. 2011; Gerlee et al. 2017; Lü et al. 2020; Xu et al. 2021; Liu et al. 2024).

A potential issue is that the addition of rule sets or new force terms may render the model cumbersome, thereby reducing its generalizability. Such models are often effective in specific scenarios, but their optimization for specific objectives may, in fact, weaken their generalization capability. In this regard, it may be more effective to develop a general model by simplifying existing models rather than by adding complexity.

In consideration of applicability and stability, the general model of the operational layer should incorporate the following characteristics:

- **Interpretability (aligned with physical logic):** dimensional consistency, scale invariance, and parameter transfer across scenarios.
- **Empirical foundations:** grounded in empirical data and aligned with pedestrian movement intuitions.
- **Principles of minimalism:** adherence to the simplest possible rules, the fewest parameters, and ease of analysis.
- **Diversity in model performance:** fundamental diagrams and pedestrian self-organization, etc.
- **Computational efficiency:** lower computational cost compared to similar models of the same type.

To this end, a general model of pedestrian dynamics is established in this paper, constructed based on binary interactions. The rules of the model, developed from first principles, were further refined in accordance with the classic social force model to enhance simulation accuracy. Additionally, this minimalist approach facilitates the analytical examination of pedestrian interactions.

2. EXPERIENCE AND INTUITION IN PEDESTRIAN INTERACTIONS

• Anisotropy of pedestrian motion space

Traditionally, the space surrounding pedestrians has been assumed to be isotropic. This method results in a potential issue: forces from various directions may produce opposing effects, causing pedestrians to maintain high speeds even in high-density situations. Such results contradict empirical observations of pedestrian fundamental diagrams (Parisi et al. 2009). Furthermore, similar models have yet to attain optimal accuracy in crowd modeling, as they demonstrate effectiveness primarily in specific contexts, such as densely packed crowds. In such cases, vision-based or attention-driven movement patterns are ineffective, and direct physical contact leads the dense crowd to approximate the behavior of a particle system.

Empirical observations of pedestrian behavior reveal that individuals primarily focus on the dynamics in front of them, largely disregarding those behind. Prior to introducing the model, the Horizontal Field of Attention (HFA, Ω) is defined. The HFA is constrained by the attentional eccentricity angle ϕ and the attentional depth h , as depicted in Fig. 1. The angle ϕ represents the angle between the boundary of the sector-shaped HFA and the pedestrian's direction of movement. The attentional depth h can theoretically extend to infinity. For the purpose of minimizing computational cost, h can be restricted to the minimum headway that allows pedestrians to maintain free motion.

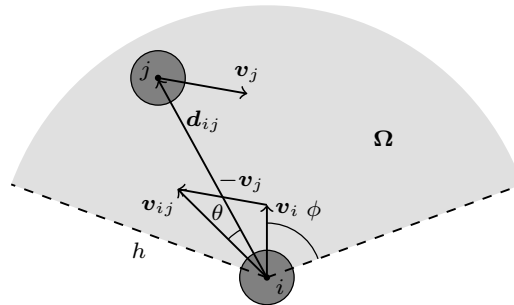


Figure 1: Diagram of the process of pedestrian interaction.

- **Pedestrians resemble elastic particles rather than rigid particles**

In the classical social force model, pedestrians are represented as rigid particles. The volume exclusion principle, which is strictly constrained by the function $g(x)$, has been shown to potentially cause distortions in pedestrian dynamics under extreme conditions. In order to capture more detailed motion dynamics, some studies have proposed the use of ellipsoidal shapes instead of circular ones to simulate pedestrian movement (Chraibi et al. 2010). On the other hand, this modification inevitably leads to an increase in model complexity. An effective compromise can be achieved by modeling pedestrians as elastic bodies rather than rigid ones. In narrow passages, pedestrians frequently turn sideways, and mutual compression between individuals reduces the space occupied. Therefore, modeling pedestrians as elastic bodies allows for a more accurate simulation of these behaviors.

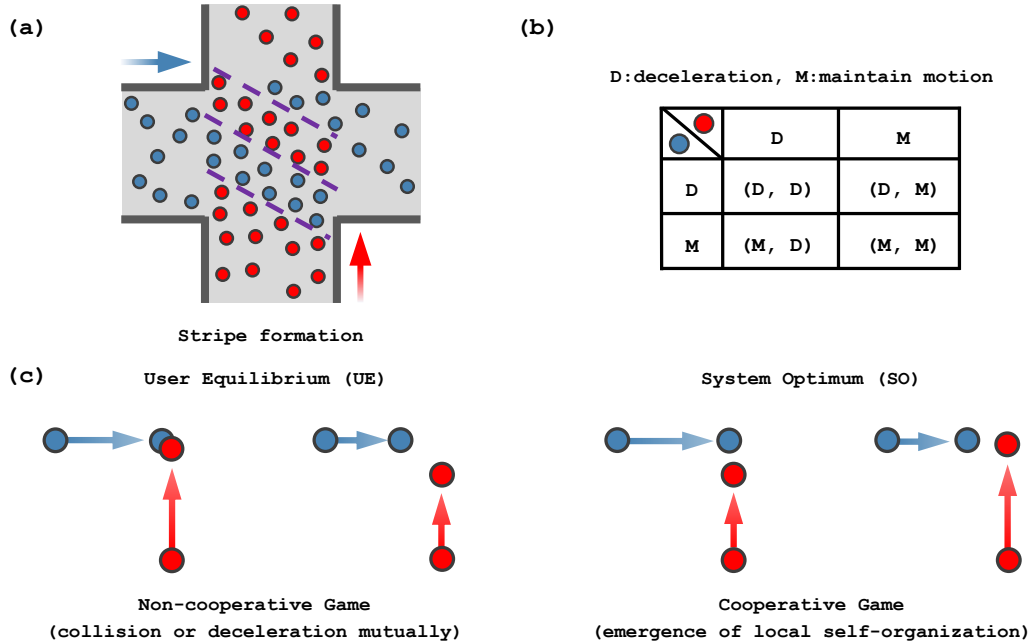


Figure 2: Scaling down the laws of stripe formation, (a) schematic diagram of stripe formation, (b) decision payoff matrix for pedestrians in binary conflicts, (c) cooperative and non-cooperative games between conflicting pedestrians.

- **Collisions are necessary**

The models based on collision avoidance algorithms has proven to be highly effective in studying interactions within crowds and is currently widely used in modeling two-dimensional multi-agent systems for obstacle avoidance (Van den Berg et al. 2008; Tordeux et al. 2016). However, a potential issue is that the precise collision avoidance algorithm actually limits its capability for high-accuracy crowd simulation: in crowds, collisions are common and, in some situations, even inevitable. This discrepancy arises mainly because pedestrian speed and movement direction are updated based on empirical estimates rather than precise numerical calculations. In reality, pedestrians can't perform such calculations, so their movements rely on rough approximations. In this consideration, the collision process is crucial for pedestrian simulation, especially in high-density crowd scenarios.

- **How many pedestrians can we tracked simultaneously?**

Research based on collective dynamics typically establishes models from a holistic perspective, wherein macro-level rules govern the evolution of groups, such as the BOID model (Reynolds 1987) and network models (Bode et al. 2011; Allen et al. 2017). Based on metrics (Vicsek et al. 1995), topological (Ballerini et al. 2008), or visual connection (Rosenthal et al. 2015; Wirth et al. 2023), the state of individuals exhibits a strong correlation with the characteristics of their surrounding neighborhoods. The complexity and variability of pedestrian dynamics hinder the approximation of crowds to fish schools or flocks of birds. However, the paradigms of interactions observed can indeed be transferred across species.

When pedestrians move within a crowd, they primarily rely on vision to acquire information. The visual field of pedestrians encompasses a considerable range, potentially including dozens or even hundreds of other pedestrians and possible obstacles. However, the range within which pedestrians actually focus their attention is quite limited.

The allocation of attention by pedestrians falls within the domains of cognitive sciences. In addition to the "magical number 4" theory (Cowan 2001) concerning visual attention, mainstream perspectives suggest that the complexity and dynamism of the environment affect the number of observable entities, with higher levels of dynamism and complexity leading to a reduction in the number of objects that pedestrians can track (Alvarez & Franconeri 2007).

In highly stochastic and dynamic crowds, pedestrians can realistically focus on only a very limited number of targets, typically the nearest neighbors within their attention field. From this perspective, models that employ binary interactions (topological connections for $n=1$) rather than metric-based interactions may be more concise and efficient.

- **Cooperative game induces local self-organization**

The phenomenon of self-organization among pedestrians is characterized by entropy reduction and the emergence of steady states within pedestrian flow systems. From a reductionist perspective, we conjecture that such entropy reduction is presumably induced by local cooperative interactions among conflicting pedestrians (Rand et al. 2014; Su et al. 2022; Bonnemain et al. 2023; Zablotsky et al. 2024). For instance, in a typical crossing flow scenario, as depicted in Fig. 2(a), there is a potential risk of collision between crossing pedestrians. Anticipation mechanism, involving a negotiation or game process, can facilitate "phase separation" between pedestrians moving in different directions. The interaction results between pedestrians from distinct directions can be represented by a simple payoff matrix, as shown in Fig. 2(b). Cooperative games contribute to entropy reduction within the system, leading to the emergence of spontaneous order, as illustrated in Fig. 2(c). In the model, the local cooperation rule is implicitly embedded via the asymmetric forces interaction based on the cosine constraint.

3. METHODOLOGY

3.1. Constraint of Space-speed Relationship

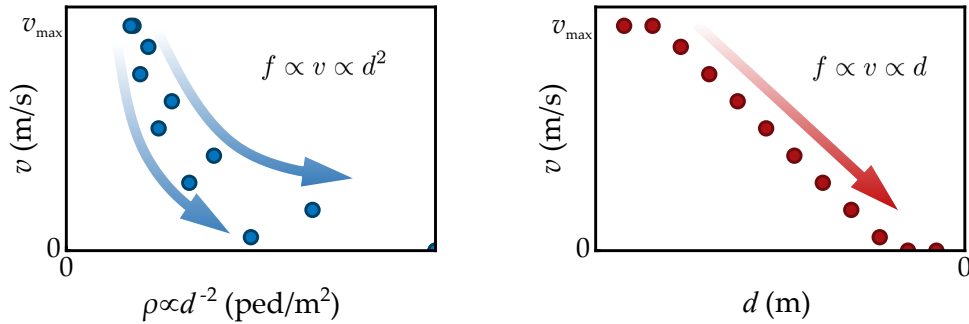


Figure 3: Space-speed relationship, (a) speed-local density constraint, (b) speed-headway constraint.

The relationship between speed and space has been extensively studied in the context of pedestrian dynamics, as illustrated in Fig. 2. Assuming isotropic pedestrian interactions, it has been shown that under constrained conditions, velocity is inversely proportional to local density (i.e., the speed–local density relationship), as expressed in Eq. 1, given a constant parameter of k . Based on this empirical relationship, within the framework of force-based models, the variation in pedestrian force with respect to spatial metrics can be described by a power function ($\partial t = \tau$), as explained in Eq. 2.

$$v \propto \rho^{-1} \propto d^2 \quad (1)$$

$$\begin{cases} \partial v = k \partial d^2 \text{ (omit } \partial t), \\ \partial f = m \frac{\partial v}{\partial t} = mk \frac{\partial d^2}{\partial t}. \end{cases} \quad (2)$$

Furthermore, in one-dimensional motion, a linear empirical relationship between the headway and speed is typically employed, often associated with the principle of constant time headway. Considering the anisotropy of the pedestrian movement space, this linear relationship, based on the nearest neighbor distance, can similarly be extended to two-dimensional motion, as illustrated in Eq. 3. In this context, a linear function can be employed to describe the variation of pedestrian force with respect to nearest neighbor relative distance ($\partial t = \tau$), as shown in Eq. 4.

$$d = vt_h + d_0 \quad \Rightarrow \quad v = \frac{d - d_0}{t_h} \quad (3)$$

$$\begin{cases} \frac{\partial d}{\partial v} = t_h \text{ (omit } \partial t), \\ \frac{\partial f}{\partial v} = \frac{m \partial v}{\partial t} = \frac{m \partial d}{t_h \partial t}. \end{cases} \quad (4)$$

Within the framework of force-based models, based on these property, it is natural to employ power functions or linear functions of distance to describe such mechanisms. The empirical formulas underlying linear functions demonstrates dimensional consistency and scale invariance, contributes to its stability.

Based on the hypothesis of binary interactions, each pedestrian in a non-collision condition both subject to only two forces: the self-driving force and the nearest-neighbor repulsive force. Consequently, the equilibrium properties of pedestrians in a one-dimensional scenario can be derived as follows:

$$v \rightarrow \max \left(\min \left(\frac{d_{ij} - r_{ij}}{t_h}, v_{\max} \right), 0 \right) \Rightarrow f_{ij} \rightarrow f_i. \quad (5)$$

The scalar form of the self-driving force f_i is defined by Eq. 6. Therefore, the equation for the nearest-neighbor repulsive force at equilibrium can be expressed as shown in Eq. 7.

$$f_i = \frac{m_i}{\tau} (v_{\max} - v_i) \quad (6)$$

$$f_{ij} = \frac{m_i}{\tau} \left(v_{\max} - \max \left(\min \left(\frac{d_{ij} - r_{ij}}{t_h}, v_{\max} \right), 0 \right) \right) \quad (7)$$

3.2. Anticipation and reaction mechanisms within force-based model framework

• Collision avoidance based on $\cos\theta$

In the computation based on two-dimensional TTC, the angle θ between the relative velocity and relative distance plays a critical role in pedestrians' collision avoidance processes ($\cos\theta$ represents the projection scale between the relative velocity and relative distance). An additional scaling factor $(1 + \alpha \cos\theta)$ is introduced into the nearest-neighbor repulsive force to describe the effect of collision avoidance. Here, α is a dimensionless coefficient that regulates the collision avoidance scale of pedestrians, satisfying $(1 + \alpha \cos\theta) \in [1 - \alpha, 1 + \alpha]$. $\alpha \rightarrow 0$ indicates that pedestrians are insensitive to collisions, which typically corresponds to unidirectional flow scenarios. $\alpha \rightarrow 1$ signifies that pedestrians are highly sensitive to collisions, corresponding to crowd or multiphase flow scenarios.

• Symmetric and Aymmetric forces

Based on the HFA described above, pedestrian interactions involve both reciprocal and non-reciprocal interactions, as illustrated in Fig. 4. Symmetric and asymmetric forces naturally be employed to represent these mechanisms. Overall, these mechanisms are associated with the anticipation and reaction behaviors observed in pedestrian dynamics. In this context, the anticipation mechanism is referred to as a implicit cooperative game process among conflicting pedestrians (inducing separation). Conversely, the reaction mechanism is described as the convergence process among co-directional pedestrians (inducing aggregation).

3.2.1. Individual-level analysis

The nearest-neighbor interaction force \mathbf{f}_{ij} is adjusted nonlinearly using a cosine function of the angle θ . When $\theta \rightarrow 0$, it indicates a potential collision trend, and \mathbf{f}_{ij} increases. When $\theta \rightarrow \pi$, it indicates a separation trend between pedestrians, and \mathbf{f}_{ij} decreases. With the introduction of the cosine function, the phenomena of separation and aggregation have been implicitly simulated.

• Separation of conflicting flows

Fig. 4(c) shows two agents, i and j , in a cross-flow scenario with a potential collision, subject to mutually repulsive forces. Since agent j is closer to the conflict point, the velocity reduction due to the repulsive force is smaller ($\|\mathbf{f}_{j,i,x}\| < \|\mathbf{f}_{i,j,y}\|$). This trend is gradually amplified with the update of their relative positions, ultimately leading to agent i yielding to agent j (cooperative game). Strictly speaking, if the agents' radii are ignored, non-cooperative games occur only when $\theta = 0$.

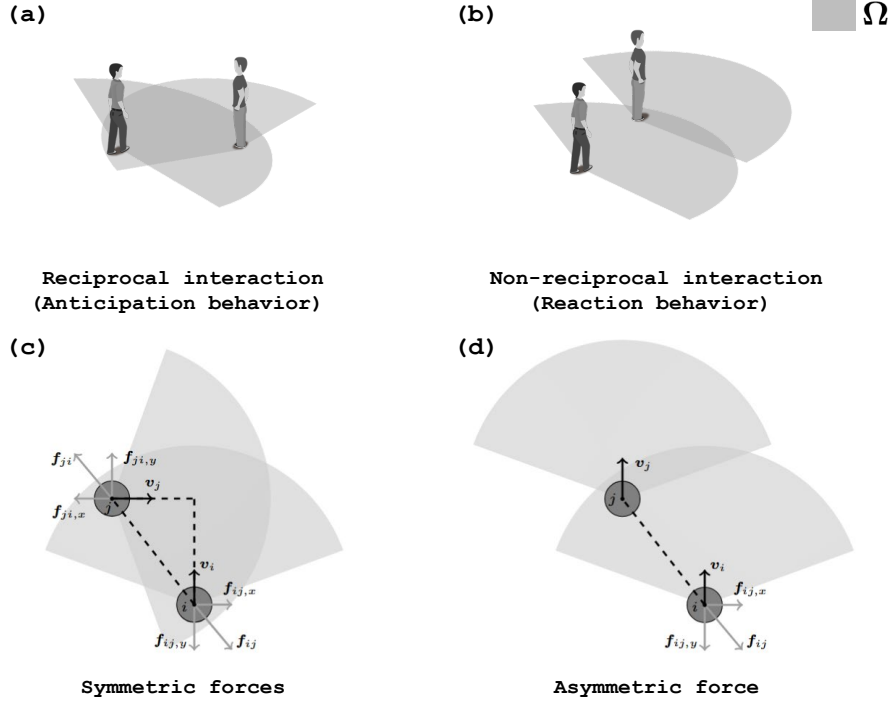


Figure 4: Schematic of nearest neighbor interaction: (a) reciprocal interaction (anticipation mechanism), (b) non-reciprocal interaction (reaction mechanism).

• Aggregation of co-directional flows

Fig. 4(d) illustrates that in unidirectional flow, agent i is subjected to the repulsive force from agent j . If $\|\mathbf{v}_j\| > \|\mathbf{v}_i\|$, \mathbf{f}_{ij} increases, and \mathbf{v}_i decreases. If $\|\mathbf{v}_j\| < \|\mathbf{v}_i\|$, \mathbf{f}_{ij} decreases, and \mathbf{v}_i increases (considering the self-driving force). This leads to the aggregation of pedestrians in the same direction. Meanwhile, it satisfies the speed-density relationship under the constraints of the fundamental diagram.

3.2.2. Analytical Analysis of the Nearest Neighbor Repulsive Force

Based on the aforementioned deduce, we derived the equation of the nearest-neighbor repulsive force as a function of distance d and angle θ , as shown in Eq. 8.

$$\mathbf{f}_{ij} = \frac{m_i}{\tau} \left(v_{\max} - \max \left(\min \left(\frac{d_{ij} - r_{ij}}{t_h}, v_{\max} \right), 0 \right) \right) (1 + \alpha \cos \theta) \quad (8)$$

For the convenience of differential computation, the tanh function can be employed to describe its continuous form, which aligns with the formulation used to represent the desired velocity in traffic flow. The continuous form is provided in Eq. 9.

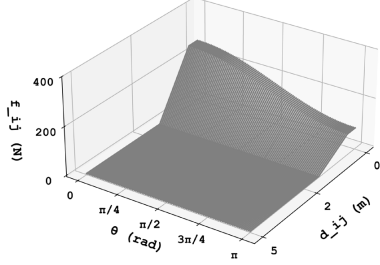
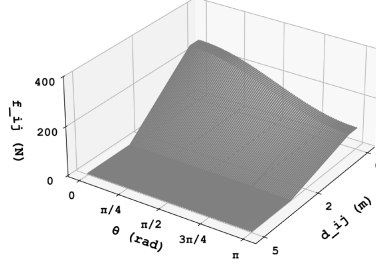
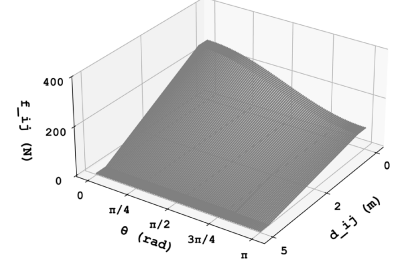
$$\mathbf{f}_{ij} = \frac{m_i}{\tau} \left(v_{\max} \left(1 - \tanh \left(\frac{d_{ij} - r_{ij}}{t_h} \right) \right) \right) (1 + \alpha \cos \theta) \quad (9)$$

Fig. 5 presents the influence of the nearest-neighbor relative distance d and angle θ on the force term. Empirical results can be used for surface fitting to investigate a more specific relationship, which may not follow a cosine function.

3.3. Model Rules

Based on the framework of a force-based model, the model is characterized by a self-driving force, a repulsive force derived from the space-speed constraint, and the contact forces that arise during collisions. Based on the assumption of binary interaction, only the force \mathbf{f}_{ij} , exerted by the nearest entity (pedestrian or wall) j ($j \in \Omega := \|\mathbf{d}_{ij}\| < h \wedge \angle(\mathbf{v}_i, \mathbf{n}_{ij}) < \phi$), is considered. The global constraints can be expressed as follows:

$$f_{ij} = \frac{m_i}{\tau} \left(v_{\max} - \max \left(\min \left(\frac{d_{ij} - r_{ij}}{t_h}, v_{\max} \right), 0 \right) \right) (1 + \alpha \cos \theta)$$

(a) $t_h=1s$ (b) $t_h=2s$ (c) $t_h=3s$

$$f_{ij} = \frac{m_i}{\tau} \left(v_{\max} \left(1 - \tanh \left(\frac{d_{ij} - r_{ij}}{t_h} \right) \right) \right) (1 + \alpha \cos \theta)$$

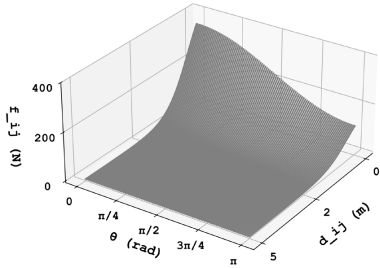
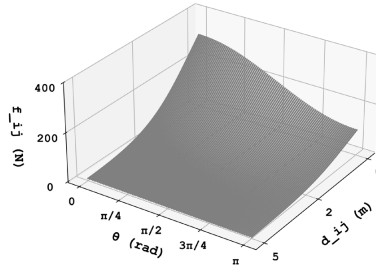
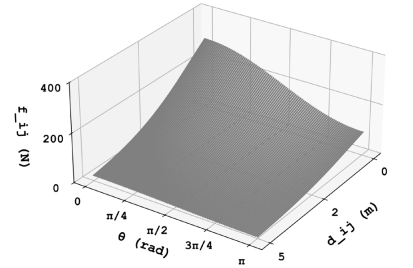
(a) $t_h=1s$ (b) $t_h=2s$ (c) $t_h=3s$

Figure 5: Relationship between the repulsive force and d and θ , ($\alpha = 0.5$), above: piecewise function, below: continuous function.

$$\mathbf{f} = \mathbf{f}_i + \mathbf{f}_{ij} + \sum_{\|\mathbf{d}_{ij}\| < r_{ij}} \mathbf{f}_c = m\mathbf{a} \quad (10)$$

Here, \mathbf{f} represents the net force acting on a target pedestrian, \mathbf{f}_i denotes the self-driving force of the pedestrian, \mathbf{f}_{ij} represents the repulsive force from the nearest neighbor j .

The self-driving force is driven by the maximum velocity vector \mathbf{v}_{\max} , expressed as:

$$\mathbf{f}_i = \frac{m_i}{\tau} (\mathbf{v}_{\max} - \mathbf{v}_i) \quad (11)$$

Here, τ represents the relaxation time, and m_i denotes the mass of pedestrian i .

The interaction force between a pedestrian and the nearest pedestrian is represented by the repulsive force, which is expanded in both piecewise and continuous forms as Eqs. 12 and 13:

Piecewise function:

$$\mathbf{f}_{ij} = \frac{m_i}{\tau} \left(\|\mathbf{v}_{\max}\| - \max \left(\min \left(\frac{\|\mathbf{d}_{ij}\| - r_{ij}}{t_h}, \|\mathbf{v}_{\max}\| \right), 0 \right) \right) (1 + \alpha \cos \theta) \mathbf{n}_{ij} \quad (12)$$

Continuous function:

$$\mathbf{f}_{ij} = \frac{m_i}{\tau} \left(\|\mathbf{v}_{\max}\| \left(1 - \tanh \left(\frac{\|\mathbf{d}_{ij}\| - r_{ij}}{t_h} \right) \right) \right) (1 + \alpha \cos \theta) \mathbf{n}_{ij} \quad (13)$$

Here, The angle θ is the angle between the relative distance and the relative velocity, $\theta = \angle(\mathbf{v}_{ij}, \mathbf{d}_{ij}) \in [0, \pi]$. Other symbols are defined as follows: $r_{ij} = r_i + r_j$, $\mathbf{v}_{ij} = \mathbf{v}_i - \mathbf{v}_j$, and $\mathbf{d}_{ij} = \mathbf{x}_j - \mathbf{x}_i$, $\mathbf{n}_{ij} = -\mathbf{d}_{ij} / \|\mathbf{d}_{ij}\|$. The simulation utilizes the difference calculation, with the nearest-neighbor repulsive forces constructed using a piecewise function.

In this process, obstacles are modeled as stationary pedestrians and are therefore included in the calculation of the repulsive force without requiring any additional rules. Different from the point-to-point interaction between pedestrians, the interaction between pedestrians and obstacles follows a point-to-line relationship. To account for all potential collision scenarios, the attentional eccentricity angle ϕ is set to a constant value of $\pi/2$.

The collision force between pedestrians is described by an exponential decay term, which is activated when the condition $\|\mathbf{d}_{ij}\| < r_{ij}$ is satisfied, as follows:

$$\mathbf{f}_c = e^{-\frac{r_{ij} - \|\mathbf{d}_{ij}\|}{\lambda}} \mathbf{n}_{ij} \quad (14)$$

The parameter settings are presented in Tab. 1, where $m = 20$ kg, $r = 0.2$ m, $\tau = 0.5$ s, $t_h = 1.3$ s, and $\lambda = 0.8$ are global parameters that remain constant across all simulations. The parameters v_{\max} , ϕ , and α will be adjusted as required. The frequency for all simulations is set as 30 FPS, corresponding to a difference time of 1/30 s.

Table 1: Parameter Descriptions and Reference Values

Parameter	Description	Reference value
m	Mass	60 kg
v_{\max}	Maximum speed	1.4 m/s
r	Radius	0.2 m
τ	Relaxation time	0.5 s
t_h	Approximate time headway	1.3 s
ϕ	Attentional eccentricity angle	[0 - π] rad
λ	Dimensionless coefficient	0.8/0.02 (scale in centimeters/meters)
α	Dimensionless coefficient	[0-1]

3.4. 1-D dynamics of CosForce model

• Approximated 2-D FVD Model under Force-based Modeling Framework

We have presented the two-dimensional form of the CosForce model to facilitate the analysis of the model's properties. The one-dimensional equation of the CosForce model is expressed as:

$$f = m_i a = \frac{m_i}{\tau} \left(\max \left(\min \left(\frac{d_{ij} - r_{ij}}{t_h}, v_{\max} \right), 0 \right) - v \right) (1 + \alpha \operatorname{sgn}(v_{ij})) \quad (15)$$

It is clear that the one-dimensional CosForce model is very similar to the FVD model (Jiang et al. 2001). The difference is that the proportional coefficient does not undergo the same scale transformation as the velocity difference. For the sake of formal consistency, $1 + \alpha \cos \theta$ can be expressed as $1 + \alpha \frac{\|\mathbf{v}_{ij} \cos \theta\|}{\|\mathbf{v}_{\max}\|}$. Thus, the one-dimensional dynamical form is reformulated from $1 + \alpha \operatorname{sgn}(v_{ij})$ to the form of $1 + \alpha \frac{v_{ij}}{v_{\max}}$. Such modifications, while increasing the complexity of the rules, were not found to lead to the anticipated improvement in model performance. The main issue lies in the inconsistency properties of speed differences between pedestrians and traffic: in traffic, a small speed difference is indicative of a stable flow state, whereas in crowds, a small speed difference may be interpreted as collective deceleration due to conflicts.

• 2-D OV model, when $\alpha = 0$

When $\alpha = 0$, the one-dimensional equation is given by Eq. 16, which is consistent with the OV model (Bando et al. 1995), the only difference being the empirical formula for the desired velocity.

$$f = m_i a = \frac{m_i}{\tau} \left(\max \left(\min \left(\frac{d_{ij} - r_{ij}}{t_h}, v_{\max} \right), 0 \right) - v \right) \quad (16)$$

4. NUMERICAL VALIDATION

In this section, we observe some fundamental constraint relationships of pedestrians. The simulated scenarios include single-file motion and unidirectional flow. The variable parameters set as follows: $v_{\max} = 1.4$ m/s, $\phi = \pi/3$, and $\alpha = 0$.

4.1. single-file pedestrians

First, we simulated the single-file motion in a channel under periodic boundary conditions, as shown in Fig. 6. Due to $\alpha = 0$, the model behaves identically to the OV model. We set $N=10, 20, 30$, and 40 in the simulation to observe the dynamics of single-file pedestrians under different densities. The pre-simulation time was 900 steps, equivalent to 30 s, and simulation data for 60 s was obtained after the pre-simulation.

From the time-space diagram in Fig. 6, it can be observed that, as the global density increases, the pedestrian flow transitions through free flow, synchronized flow, and stop-and-go phases, and the traffic flow states remain highly stable.

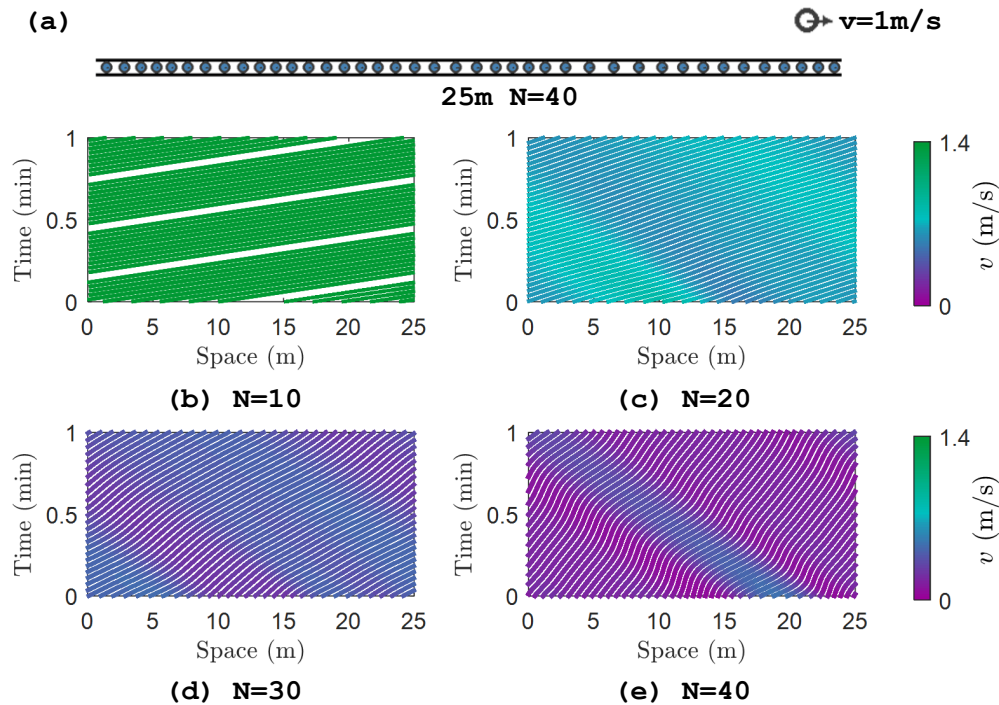


Figure 6: Simulation of single-file pedestrians: (a) simulation snapshot, (b)-(d) time-space diagram at different densities.

4.2. unidirectional flow

Similarly, we conducted simulations of pedestrian unidirectional flow scenarios in a channel with periodic boundary conditions, as shown in Fig. 7. In the simulations, we incrementally set the number of pedestrians to 10 per simulation, conducting a total of 16 simulations covering scenarios from $N = 10$ to $N = 160$. The pre-simulation time was set to 900 time steps, corresponding to 30 s, and simulation data was obtained for 100 time steps (approximately 3.33 seconds) after the pre-simulation. Fig. 7 illustrates the state constraints of unidirectional pedestrian flow, including density versus speed, headway versus speed, and angular velocity versus speed. Due to the consistent sampling time, data obtained from high-density simulations are significantly more abundant than those from low-density simulations, leading to an uneven distribution of data in the plots.

Density versus Speed

Fig. 7(c) presents the relationship between pedestrian speed and local density, which conforms to the characteristics of the pedestrian speed-density curve, showing an inverse proportional relationship in non-free-flow conditions.

Headway versus Speed

Fig. 7(d) illustrates the relationship between pedestrian speed and the nearest neighbor relative distance, with the distribution trend aligning with empirical results. Specifically, under non-free-flow conditions, speed exhibits a linear

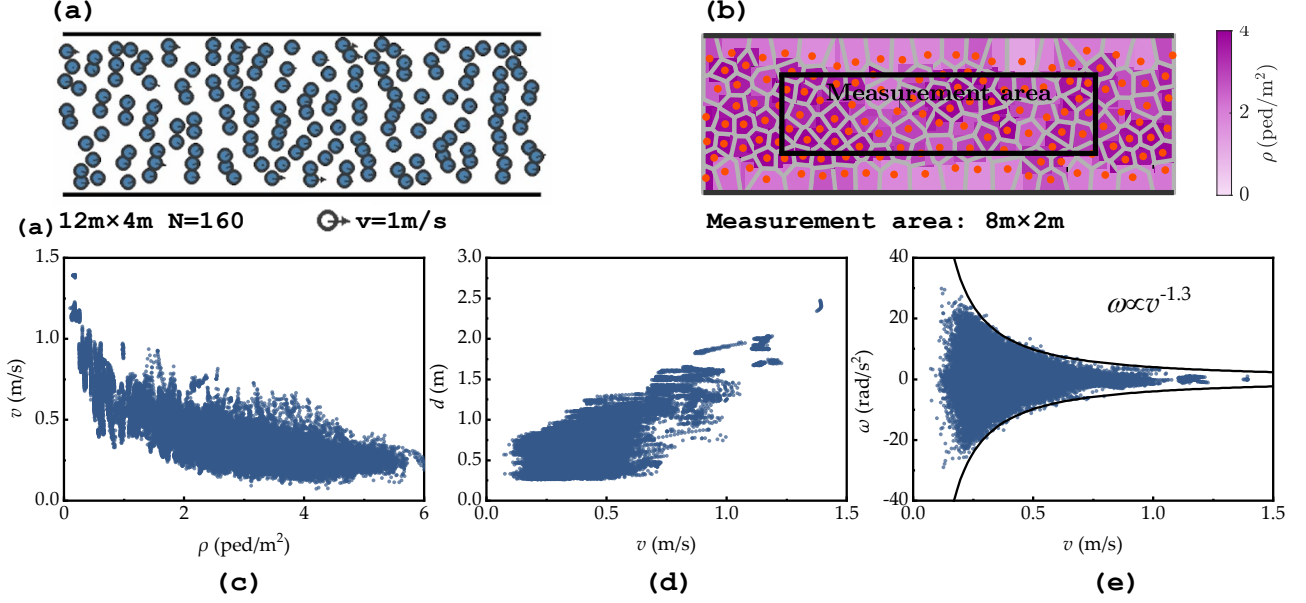


Figure 7: Simulation of uni-directional pedestrian flow, (c)-(d) show the constraint relationships of the basic properties.

relationship with the nearest neighbor distance. The model is constructed based on a linear space-speed constraint, this result hence reasonably meets our expectations.

Angular velocity versus Speed

Fig. 7(e) shows the relationship between pedestrian angular velocity and speed, with the maximum angular velocity constraint exponent approximately equal to -1.3, slightly lower than our previous empirical observation (where the maximum angular velocity constraint exponent is -0.8, approximately).

5. "PHASE SEPARATION" IN CROWDS

In crowd dynamics, "phase separation" refers to the phenomenon where separation occurs between groups with different directions or states, induced by spontaneous order. Common examples include lane formation, stripe formation, and cross-channel formation. However, effective metrics for quantitatively estimating self-organization phenomena in crowds are still limited. Based on the mechanisms of self-organization: entropy reduction and steady state, we propose 3 quantitative analytical metrics: the average normalized velocity $\langle v \rangle$, the variance of normalized speed $Var(v)$, and the entropy of normalized speed H , with their formulas provided in Eqs. 17-19. These metrics provide quantitative standards for the efficiency of crowd movement, the volatility of crowd speed, and the degree of chaos in the crowd, respectively.

$$\langle v \rangle = \sum_{i \in N} \frac{\|\mathbf{v}_i\|}{N v_{\max}} \quad (17)$$

$$Var(v) = Var\left(\frac{\|\mathbf{v}_{i \in N}\|}{v_{\max}}\right) \quad (18)$$

$$H = - \sum_{j=1}^{10} p(\langle v_{i \in N} \rangle_j) \log(p(\langle v_{i \in N} \rangle_j)) \quad (19)$$

The simulation environment is set as an 8m x 8m with fully periodic boundary conditions. Snapshots of the three scenarios are shown in Fig. 8. In the initial state, all pedestrians are uniformly distributed, with an initial velocity of 0. The simulation time for a single scenario is 3000 steps (100 seconds).

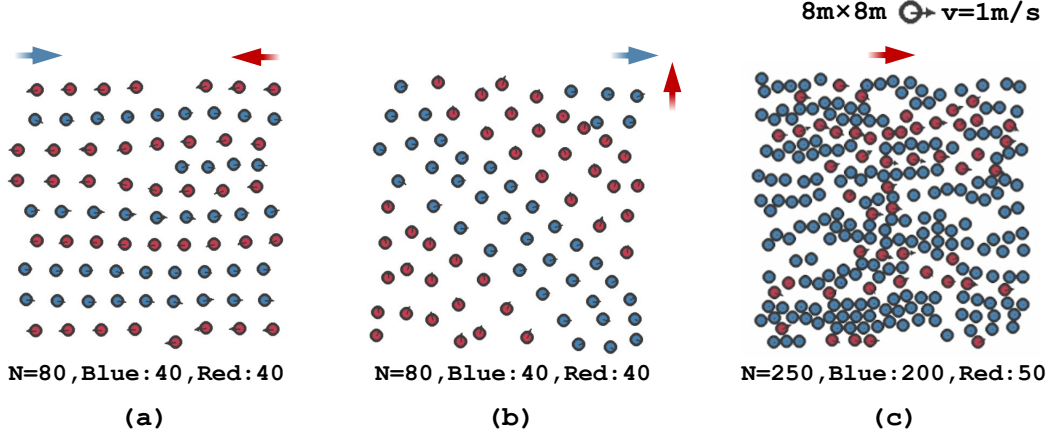


Figure 8: Simulation snapshots of pedestrian "phase separation": (a) lane formation, (b) stripe formation, (c) cross-channel formation.

5.1. Lane formation

First, we performed simulations of the lane-formation phenomenon in bidirectional pedestrian flows. The total number of pedestrians was set to 80, with a 40 : 40 directional configuration. The variable parameters were set as $v_{\max} = 1.4 \text{ m/s}$, $\phi = \pi/2$, and $\alpha = 0.5$. We conducted 10 independent simulations, and the resulting trends of the average normalized speed, the variance of normalized speed, and the entropy of normalized speed are shown in Fig. 9.

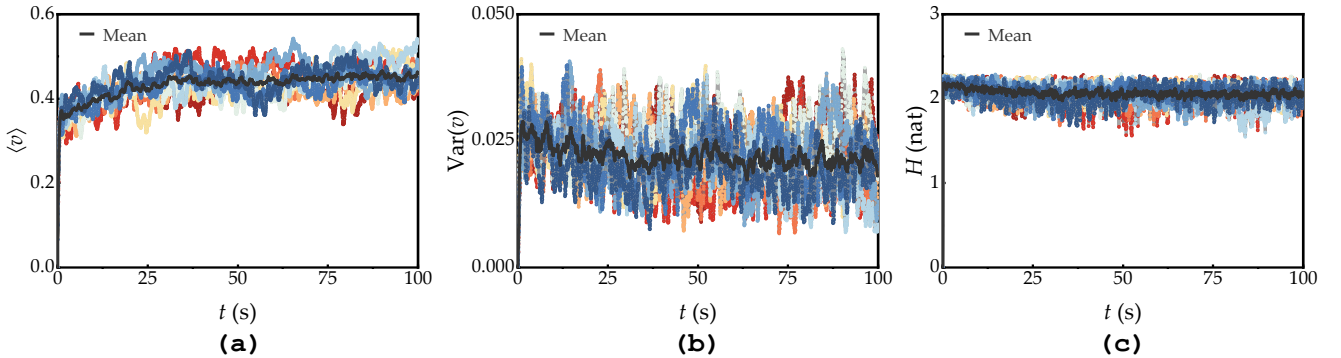


Figure 9: Variation of crowd velocity metric over time: (a) average normalized speed, (b) variance of normalized speed, (d) entropy of normalized speed.

Fig. 9 shows that within a short initial period (approximately 30 seconds), the average normalized speed increases and reaches a stable state, maintaining an average value of approximately 0.6 m/s. Correspondingly, the variance and entropy of the normalized speeds are also observed to decrease and stabilize.

5.2. Stripe formation

Also, we conducted a simulation of the stripe-formation phenomenon in cross pedestrian flow. The total number of pedestrians was set to 80, with a directional configuration of 40 : 40. The variable parameters were set as $v_{\max} = 1.4 \text{ m/s}$, $\phi = \pi/3$, and $\alpha = 0.5$. 10 independent simulations were performed, and the trends of the average normalized speed, the variance and entropy of normalized speed are presented in Fig. 10.

Fig. 10 presents a trend similar to that in Fig. 9, i.e., the decrease in the average speed is accompanied by a reduction in both the speed variance and entropy. In terms of the changes in the mean, this trend is observed to be quite steady. Such properties indicate the process of spontaneous order formation within the system, and this formation of order typically occurs within a time frame ranging from several seconds to a few tens of seconds.

5.3. Cross-channel formation

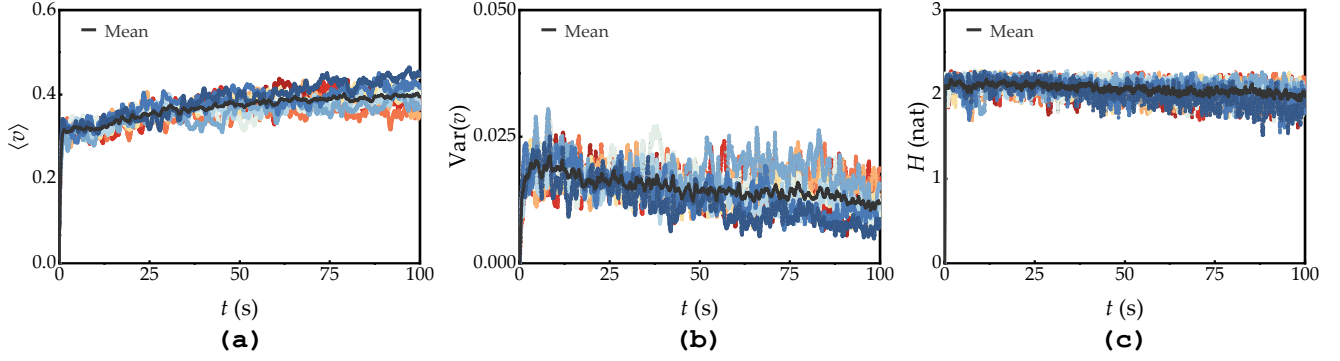


Figure 10: Variation of crowd velocity metric over time: (a) average normalized speed, (b) variance of normalized speed, (d) entropy of normalized speed.

The final scenario in the simulation of phase separation is referred to as "cross-channel formation", which describes the phenomenon where pedestrians, when crossing through high-density and low-dynamics crowds, form a series of stable crossing channels. A field video of such phenomenon in a train station can be seen in (Wang 2024). In our simulations, the total number of pedestrians was set to 250, with a proportionally varied pedestrian state configuration (dynamic and static). The variable parameters were set as $v_{\max} = 1.4$ m/s (dynamic) or 0 m/s (static), $\phi = \pi/2$ (dynamic) or π (static), and $\alpha = 0.5$.

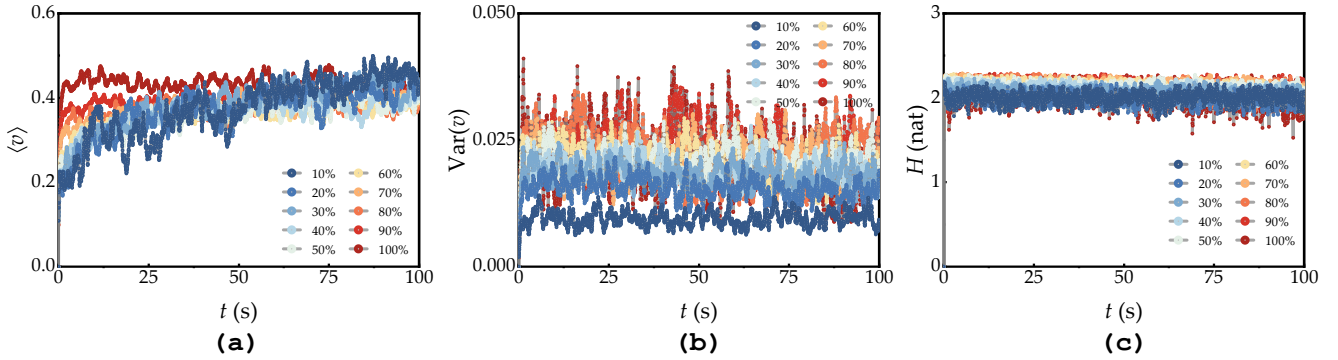


Figure 11: Variation of crowd velocity metric over time: (a) average normalized speed, (b) variance of normalized speed, (d) entropy of normalized speed.

10 independent simulations were conducted corresponding to different dynamic pedestrian ratios. The resulting trends of the average normalized speed, as well as the variance and entropy of normalized speed, are shown in Fig. 11. The configuration with a 100% dynamic pedestrian ratio can be considered as the control group, representing the unified unidirectional flow of the crowd.

From Fig. 11, we can still observe similar self-organization trends, namely, the crowd's speed steadily increases, while the speed variance and speed entropy show a stable decreasing trend.

6. "CATFISH EFFECT" IN CROWDS

The continuous dynamics of crowds are one of the fundamental causes of crowd crush. Some basic characteristics of crowd stability have been empirically observed, with contributions from pioneering work (Gu et al. 2024; Ma et al. 2013; Echeverría-Huarte et al. 2022) on the oscillation phenomenon within crowds. The sensitivity of pedestrians to spatial variations was revealed in our previous work. In general, people seem reluctant to stop, indicating that pedestrians strive to maintain dynamic, resulting in low velocities and high angular velocities.

To simulate similar mechanisms, The variable parameters were set as $v_{\max} = 1.4$ m/s $[1, 0]$ (active) or 0.6 m/s $[0, 0]$ (passive), $\phi = \pi/2$ (active) or π (passive), and $\alpha = 0.5$. The vector $[0, 0]$ represents the direction of the maximum velocity. According to Eqs. 11 and 12, under these parameter settings, the self-driven force aims to slow down

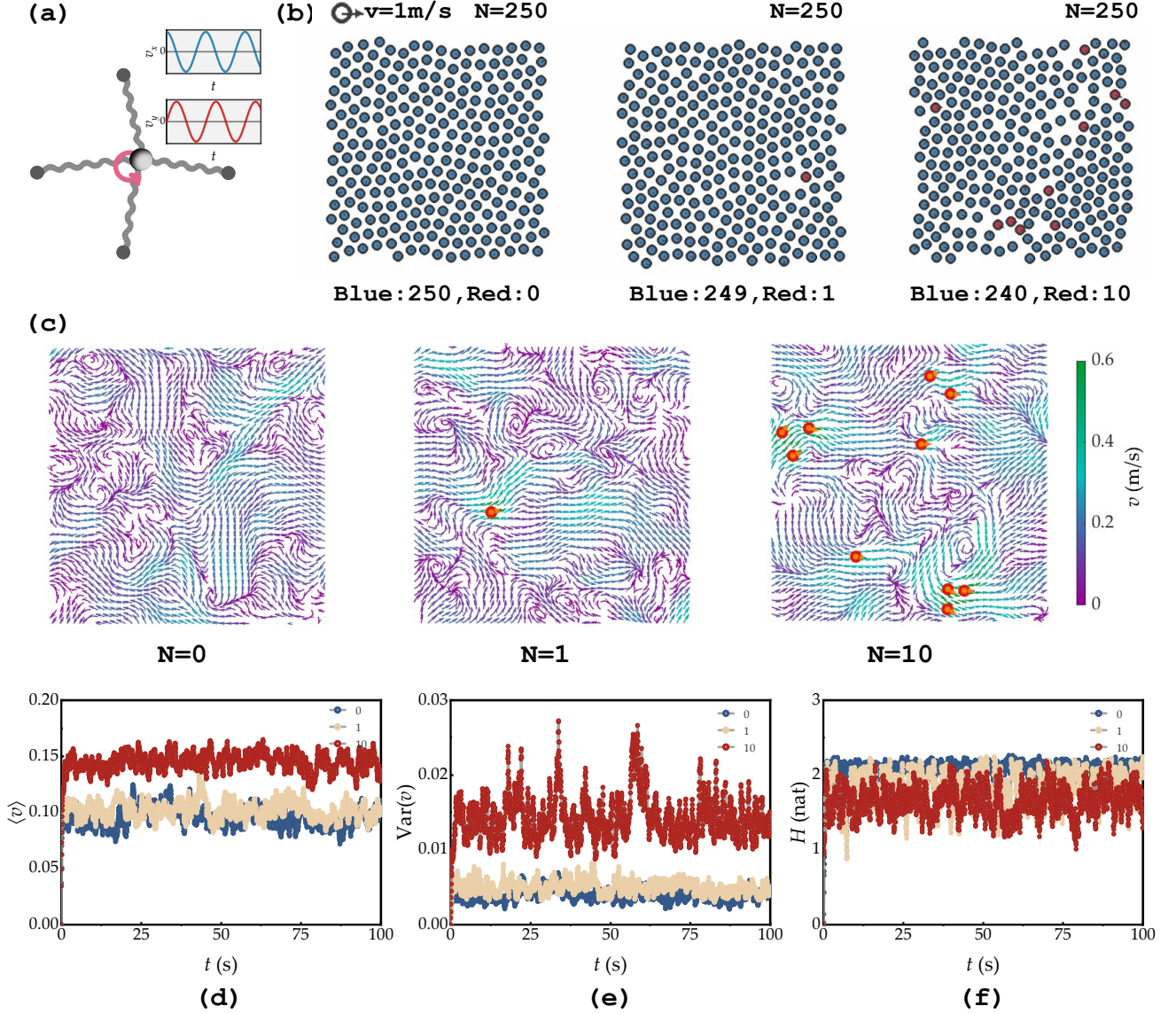


Figure 12: Simulation of the "catfish effect" in crowds: (a) physical illustration of the background crowd, (b) simulation snapshots when the number of active pedestrians is 0, 1, and 10, (c) velocity field distribution when the number of active pedestrians is 0, 1, and 10, (d)-(f): variation of speed metric over time.

pedestrians to a velocity of 0, while the repulsive force term corresponds to a maximum speed of 0.6 m/s. This setup leads to pedestrians being highly sensitive to spatial variations in the motion space and leads to a structured distribution, which is characteristic of dynamic crowds. To investigate the "catfish effect" in dynamic crowds, we added 1 and 10 "active pedestrians" in the comparative groups, with a velocity set to $v_{\max} = 1.4 \text{ m/s} [1, 0]$.

Overall, the background crowd consists of "passive pedestrians", providing the system's background environment. Our aim is to study the changes in the system state caused by the "active pedestrians" and explore the potential phenomenon of the "catfish effect", which originates from our earlier conjecture (Wang et al. 2023). The simulation environment is set as an $8\text{m} \times 8\text{m}$ with fully periodic boundary conditions. Snapshots of the three scenarios are shown in Fig. 8. In the initial state, all pedestrians are uniformly distributed, with an initial speed of 0 m/s. The simulation time for a single scenario is 3000 steps (100 s).

The background crowd is shown in Fig. 12(b) and exhibits the following characteristics:

- A closed system (full periodic boundary conditions),

- No friction,
- Collisional forces are symmetric,
- Rules lead to a structured distribution of pedestrians (asymmetric forces, being statistically symmetric, result in negligible external net forces).

These properties indicate that the system is close to momentum conservation. The trends of the orthogonal direction and the mean scalar velocity are shown in Fig. 13(a). Based on these properties, Fig. 12(a) provides an equivalent physical system for the background crowd, which is a closed system composed of four fixed points constrained by Hookean springs and balls, where the balls undergo uniform circular motion.

In the comparative scenarios, 1 and 10 "active pedestrians" were added, respectively. Fig. 12(c) shows the distribution of the velocity field, with the corresponding quantitative data presented in Figs. 12(d)-12(f). From the statistical data, after the introduction of polarized "active pedestrians", the system's kinetic energy showed an increment, accompanied by a larger variance of speed. However, an intriguing phenomenon is that the entropy of velocity decreases. The underlying reasons remain unexplained. These results suggest that the presence of "active pedestrians" enhances the ordering of the dynamic crowd.

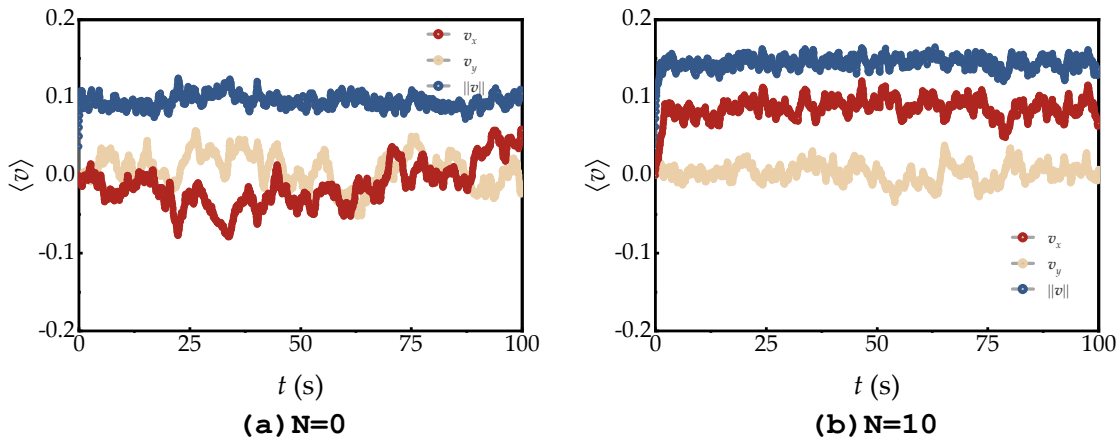


Figure 13: Average orthogonal velocity and scalar speed over time for the number of "active pedestrians": (a) $N = 0$, (b) $N=10$.

From the perspective of momentum analysis, we examined the orthogonal velocity distribution when the number of "active pedestrians" was 0 and 10, respectively. In the control group, the velocity component in the orthogonal direction fluctuated around zero, indicating that the system was near equilibrium. In Fig. 13(b), the inclusion of "active pedestrians" led to a polarization effect in the x -direction, resulting in an increase in the average normalized speed in the x -direction by approximately 0.1. From the perspective of momentum variation, the momentum increment of the 10 "active pedestrians" did not exceed 10 units (assuming uniform pedestrian mass and a normalized maximum speed of 1), while the average velocity in the x -direction increased by approximately 0.1, corresponding to a total momentum gain of about 25 units in the system. The fluctuation trend in the y -direction velocity remained consistent with that of the control group.

Referring to Fig. 12(c), we observed that the momentum in different directions within the control group canceled each other out, leading to a small total momentum that fluctuated around zero. When the "active pedestrians" entered the crowd, adjacent individuals gradually adjusted their velocity, and the random momentum became more organized (i.e., polarized), resulting in a significant increase in the system's total momentum (gain > increment).

7. LIMITATIONS

In the simulation, we also explored the limitations of the model, which mainly include two aspects:

- **Inability to simulate tactical-level behaviors:** As shown in Fig. 13 (a) and (b), even simulating some local tactical-level behaviors, such as short-term route decisions, is beyond the capability of the model, which is a common limitation of most operational-level models.

• **Distortion in response to static environments:** In certain static environments, pedestrians may become trapped even when space is available. Within the framework of force-based models, there exist equilibrium positions in static environments that cause the pedestrian's force balance, resembling a black hole, where pedestrians passing nearby will draw towards these equilibrium points.

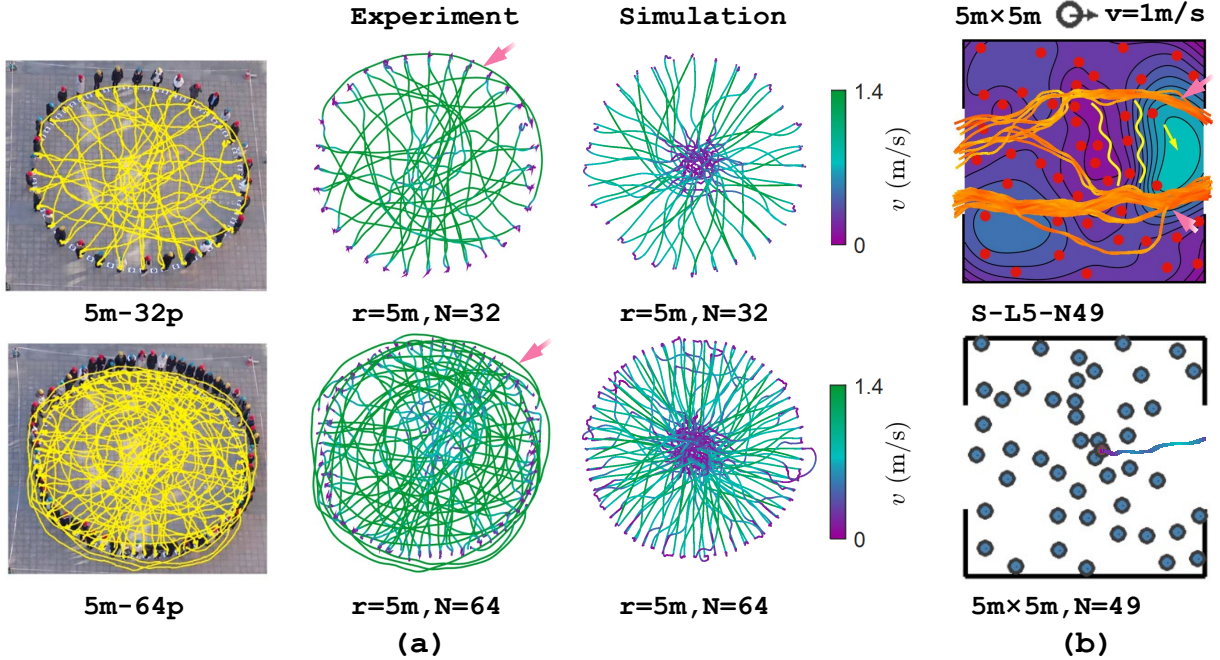


Figure 14: Limitations of the model: comparison between experimental and simulation trajectories. (a) antipode experiment, (b) crowd-cross experiment (static).

8. CONCLUSIONS

In this paper, we propose a force-based general model, CosForce. The model consists of 8 parameters (6 agent state parameters and 2 dimensionless coefficients), along with four equations.

In order to simulate pedestrians' anticipation and reaction behaviors, as well as the associated collision avoidance mechanisms, symmetric and asymmetric forces constrained by cosine functions are employed. Despite its simplicity, the model demonstrates effective performance, being capable of simulating a range of pedestrian self-organization phenomena, among others.

We explored "phase separation" and the "catfish effect" within crowds based on simulations of the CosForce model. First, several quantitative metrics were introduced to evaluate pedestrians' self-organization process, including the average normalized speed, the variance of normalized speed, and the entropy of normalized speed. Given that the theory of pedestrian self-organization is well-established and supported by empirical observations, the simulation results align with our expectations. On the other hand, the simulation of the "catfish effect" within crowds is entirely theoretical. A key finding is that while "active pedestrians" contribute to an additional gain in system momentum, the system's entropy of speed decreases, simultaneously. In our simulation, "active pedestrians" induce the formation of order within the crowd. The rules governing pedestrian motion are simple and reasonable, with the desired speed derived from an empirical equation that ensures dimensional consistency. We consider the results valid. In summary, further discoveries rely on additional exploration, particularly through empirical observations.

Theoretically, compared to traditional force-based models, the complexity of the CosForce model can be reduced from $O(n^2)$ to $O(n)$. Currently, we are pursuing this via a structured calculation method.

DATA AVAILABILITY

The code can be found at: https://drive.google.com/drive/folders/1NYVnRp0z8VPuskfezMr51gB-sraOf6Iq?usp=drive_link (Google Drive), and a short video summary is available at: <https://www.bilibili.com/video/BV17B1oYVEQm/>.

ACKNOWLEDGMENTS

This work was supported by the National Natural Science Foundation of China (Grant No. 52072286, 71871189, 51604204), and the Fundamental Research Funds for the Central Universities (Grant No. 2022IVA108).

REFERENCES

- Allen, B., Lippner, G., Chen, Y.-T., et al. 2017, *Nature*, 544, 227, doi: [10.1038/nature21723](https://doi.org/10.1038/nature21723)
- Alvarez, G. A., & Franconeri, S. L. 2007, *Journal of vision*, 7, 14, doi: [10.1167/7.13.14](https://doi.org/10.1167/7.13.14)
- Ballerini, M., Cabibbo, N., Candelier, R., et al. 2008, *Proceedings of the National Academy of Sciences*, 105, 1232, doi: [10.1073/pnas.0711437105](https://doi.org/10.1073/pnas.0711437105)
- Bando, M., Hasebe, K., Nakayama, A., Shibata, A., & Sugiyama, Y. 1995, *Physical review E*, 51, 1035, doi: [10.1103/PhysRevE.51.1035](https://doi.org/10.1103/PhysRevE.51.1035)
- Bode, N. W., Wood, A. J., & Franks, D. W. 2011, *Behavioral ecology and sociobiology*, 65, 117, doi: [10.1007/s00265-010-1111-0](https://doi.org/10.1007/s00265-010-1111-0)
- Bonnemain, T., Butano, M., Bonnet, T., et al. 2023, *Physical Review E*, 107, 024612, doi: [10.1103/PhysRevE.107.024612](https://doi.org/10.1103/PhysRevE.107.024612)
- Burstedde, C., Klauck, K., Schadschneider, A., & Zittartz, J. 2001, *Physica A: Statistical Mechanics and its Applications*, 295, 507, doi: [10.1016/S0378-4371\(01\)00141-8](https://doi.org/10.1016/S0378-4371(01)00141-8)
- Chraïbi, M., Seyfried, A., & Schadschneider, A. 2010, *Physical Review E*, 82, 046111, doi: [10.1103/PhysRevE.82.046111](https://doi.org/10.1103/PhysRevE.82.046111)
- Cowan, N. 2001, *Behavioral and brain sciences*, 24, 87, doi: [10.1017/S0140525X01003922](https://doi.org/10.1017/S0140525X01003922)
- Echeverría-Huarte, I., Nicolas, A., Hidalgo, R. C., Garcimartín, A., & Zuriguel, I. 2022, *Scientific reports*, 12, 2647, doi: [10.1038/s41598-022-06493-0](https://doi.org/10.1038/s41598-022-06493-0)
- Farina, F., Fontanelli, D., Garulli, A., Giannitrapani, A., & Prattichizzo, D. 2017, *PloS one*, 12, e0169734, doi: [10.1371/journal.pone.0169734](https://doi.org/10.1371/journal.pone.0169734)
- Frielink-Loing, A. F., Koning, A., & van Lier, R. 2017, *Journal of Vision*, 17, 3, doi: [10.1167/17.4.3](https://doi.org/10.1167/17.4.3)
- Gerlee, P., Tunstrøm, K., Lundh, T., & Wennberg, B. 2017, *Physical Review E*, 96, 062413, doi: [10.1103/PhysRevE.96.062413](https://doi.org/10.1103/PhysRevE.96.062413)
- Gu, F., Guiselin, B., Bain, N., Zuriguel, I., & Bartolo, D. 2024, *Bulletin of the American Physical Society*
- Guy, S. J., Chhugani, J., Curtis, S., et al. 2010, in *Symposium on computer animation*, 119–128, doi: [10.2312/SCA/SCA10/119-128](https://doi.org/10.2312/SCA/SCA10/119-128)
- Helbing, D., & Molnar, P. 1995, *Physical review E*, 51, 4282, doi: [10.1103/PhysRevE.51.4282](https://doi.org/10.1103/PhysRevE.51.4282)
- Jiang, R., Wu, Q., & Zhu, Z. 2001, *Physical Review E*, 64, 017101, doi: [10.1103/PhysRevE.64.017101](https://doi.org/10.1103/PhysRevE.64.017101)
- Katz, Y., Tunstrøm, K., Ioannou, C. C., Huepe, C., & Couzin, I. D. 2011, *Proceedings of the National Academy of Sciences*, 108, 18720, doi: [10.1073/pnas.1107583108](https://doi.org/10.1073/pnas.1107583108)
- Liu, F., Ohsita, Y., Kashima, K., et al. 2024, in *2024 IEEE International Conference on Consumer Electronics (ICCE)*, IEEE, 1–6, doi: [10.1109/ICCE59016.2024.10444159](https://doi.org/10.1109/ICCE59016.2024.10444159)
- Lü, Y.-X., Wu, Z.-X., & Guan, J.-Y. 2020, *Physical Review Research*, 2, 043250, doi: [10.1103/PhysRevResearch.2.043250](https://doi.org/10.1103/PhysRevResearch.2.043250)
- Ma, J., Song, W., Lo, S. M., & Fang, Z. 2013, *Journal of Statistical Mechanics: Theory and Experiment*, 2013, P02028, doi: [10.1088/1742-5468/2013/02/P02028](https://doi.org/10.1088/1742-5468/2013/02/P02028)
- Moussaïd, M., Helbing, D., & Theraulaz, G. 2011, *Proceedings of the National Academy of Sciences*, 108, 6884, doi: [10.1073/pnas.1016507108](https://doi.org/10.1073/pnas.1016507108)
- Parisi, D. R., Gilman, M., & Moldovan, H. 2009, *Physica A: Statistical Mechanics and its Applications*, 388, 3600, doi: [10.1016/j.physa.2009.05.027](https://doi.org/10.1016/j.physa.2009.05.027)
- Rand, D. G., Nowak, M. A., Fowler, J. H., & Christakis, N. A. 2014, *Proceedings of the National Academy of Sciences*, 111, 17093, doi: [10.1073/pnas.1400406111](https://doi.org/10.1073/pnas.1400406111)
- Renton, A. I., Painter, D. R., & Mattingley, J. B. 2019, *Cerebral Cortex*, 29, 2366, doi: [10.1093/cercor/bhy105](https://doi.org/10.1093/cercor/bhy105)
- Reynolds, C. W. 1987, in *Proceedings of the 14th annual conference on Computer graphics and interactive techniques*, 25–34, doi: [10.1145/37401.37406](https://doi.org/10.1145/37401.37406)
- Rosenthal, S. B., Twomey, C. R., Hartnett, A. T., Wu, H. S., & Couzin, I. D. 2015, *Proceedings of the National Academy of Sciences*, 112, 4690, doi: [10.1073/pnas.1420068112](https://doi.org/10.1073/pnas.1420068112)

- Su, Q., Allen, B., & Plotkin, J. B. 2022, Proceedings of the National Academy of Sciences, 119, e2113468118, doi: [10.1073/pnas.2113468118](https://doi.org/10.1073/pnas.2113468118)
- Tordeux, A., Chraïbi, M., & Seyfried, A. 2016, in Traffic and Granular Flow'15, Springer, 225–232, doi: [10.1007/978-3-319-33482-0_29](https://doi.org/10.1007/978-3-319-33482-0_29)
- Van den Berg, J., Lin, M., & Manocha, D. 2008, in 2008 IEEE international conference on robotics and automation, Ieee, 1928–1935, doi: [10.1109/ROBOT.2008.4543489](https://doi.org/10.1109/ROBOT.2008.4543489)
- Vicsek, T., Czirók, A., Ben-Jacob, E., Cohen, I., & Shochet, O. 1995, Physical review letters, 75, 1226, doi: [10.1103/PhysRevLett.75.1226](https://doi.org/10.1103/PhysRevLett.75.1226)
- Wang, J. 2024, Cross-channel formation. <https://www.bilibili.com/video/BV1eA2QYdE3C/>
- Wang, J., Lv, W., Jiang, H., Fang, Z., & Ma, J. 2023, arXiv preprint arXiv:2311.04827, doi: [10.48550/arXiv.2311.04827](https://doi.org/10.48550/arXiv.2311.04827)
- Wirth, T. D., Dachner, G. C., Rio, K. W., & Warren, W. H. 2023, PNAS nexus, 2, pgad118, doi: [10.1093/pnasnexus/pgad118](https://doi.org/10.1093/pnasnexus/pgad118)
- Xu, Q., Chraïbi, M., & Seyfried, A. 2021, Transportation research part C: emerging technologies, 133, 103464, doi: [10.1016/j.trc.2021.103464](https://doi.org/10.1016/j.trc.2021.103464)
- Yi, W., Wu, W., Wang, X., & Zheng, X. 2023, IEEE Transactions on Intelligent Transportation Systems, 24, 10108, doi: [10.1109/TITS.2023.3268315](https://doi.org/10.1109/TITS.2023.3268315)
- Zablotsky, A., Kuperman, M., & Bouzat, S. 2024, Physical Review E, 109, 054304, doi: [10.1103/PhysRevE.109.054304](https://doi.org/10.1103/PhysRevE.109.054304)
- Zanlungo, F., Ikeda, T., & Kanda, T. 2011, Europhysics Letters, 93, 68005, doi: [10.1209/0295-5075/93/68005](https://doi.org/10.1209/0295-5075/93/68005)